P1.2 SECOND- AND THIRD-ORDER VERTICAL VELOCITY BUDGETS IN CLOUDY BOUNDARY LAYERS

Jean-Christophe Golaz[1,2*] Shouping Wang[2]

[1]National Research Council.
[2]Naval Research Laboratory, Marine Meteorology Division, Monterey, California.

1. INTRODUCTION

The Naval Research Laboratory's Coupled Ocean/Atmosphere Mesoscale Prediction System (COAMPS[TM1], Hodur 1987). has been extended to perform as a large eddy simulation (LES). The extended model, referred hereafter to as COAMPS-LES, has been validated using a number of test cases representing a range of different boundary layer cloud regimes.

From our simulations of boundary layer clouds, we have derived numerically exact budgets of the second ($\overline{w'^2}$) and third moment ($\overline{w'^3}$) of the vertical velocity w. Second moment budgets have been studied fairly extensively (e.g. Moeng 1986; Cuijpers et al. 1996; de Roode and Bretherton 2003). Budgets of $\overline{w'^3}$ have comparatively received little attention. To our knowledge, the only full LES derived budget published of a cloudy boundary layer is a shallow cumulus case from Cuijpers et al. (1996). The $\overline{w'^3}$ budget is particularly interesting because $\overline{w'^3}$ provides information about the organization of the turbulence and can vary significantly from one cloud regime to another. Also, some boundary layer parameterizations now include predictive equations for $\overline{w'^2}$ and $\overline{w'^3}$ (e.g. Lappen and Randall 2001; Golaz et al. 2002), hence sparking fresh interest in higher moment w budgets.

2. MODEL DESCRIPTION

The LES model is based on COAMPS (Hodur 1987). The prognostic variables consist of the cartesian wind components (u_i, $i = 1, 2, 3$), the perturbation Exner function (π'), the dry potential temperature (θ), the water vapor and cloud water mixing ratios (q_v, q_c). The dynamics is governed by the compressible form of the Navier-Stokes equations (Klemp and Wilhelmson 1978).

The governing equations are discretized on an Arakawa C grid. Dynamical variables (u_i, π') are integrated using a leapfrog time step and second-order centered advection. The thermodynamic variables (θ, q_t, q_c) use a forward time step and second-order Bott advection (Bott 1989). A small acoustic time step is used to stably integrate the terms responsible for sound waves. Fourth order horizontal numerical diffusion with coefficient $\nu = 0.001$ and a Robert filter with coefficient 0.2 are applied to all leapfrog variables. Cloud water is formed by saturation adjustment and no drizzle is allowed to form. The subgrid-scale fluxes are computed using a Lilly-Smagorinsky local equilibrium scheme.

3. SELECTED EXPERIMENTS

Results will only be shown for two boundary layer cases consisting of a stratocumulus and a cumulus layer. The first case is a nocturnal stratocumulus case loosely based on 7 July 1987 FIRE [First ISCCP (International Satellite Cloud Climatology Project) Regional Experiment] data described in Moeng et al. (1996). The second one is a low cloud cover trade wind cumulus case based on BOMEX (Barbados Oceanographic and Meteorological Experiment) from Siebesma et al. (2003). All results presented here are time averaged over the second hour for FIRE, and over the fourth to sixth hours for BOMEX.

Mean profiles of liquid water potential temperature (θ_l), total water mixing ratio (q_t), cloud fraction and cloud water mixing ratio (q_c) are depicted in Fig. 1. The boundary layer for the FIRE stratocumulus is well mixed from the surface up to 750 m. Cloud cover is nearly solid with a maximum cloud fraction of 90 %. The cloud water mixing ratio profile is typical of a stratocumulus layer with a maximum value of 0.20 g kg^{-1} just below cloud base. The structure of the atmosphere for BOMEX is typical of a trade wind cumulus regime. It comprises a subcloud layer from the surface up to 500 m, a conditionally unstable layer from 500 to 1500 m capped by a weak inversion layer from 1500 to 2000 m. The maximum cloud fraction is less than 6 % and the layer averaged cloud water is less than 0.006 g kg^{-1}.

4. HIGHER MOMENT VERTICAL VELOCITY BUDGETS

Governing equations for the second and third moment of the vertical velocity are traditionally derived from the w momentum equation using the Reynolds rules of averaging in conjunction with incompressibility and horizontal homogeneity assumptions (e.g. Stull 1988; André et al.

*Corresponding author address: Jean-Christophe Golaz, Naval Research Laboratory, 7 Grace Hopper Avenue Stop 2, Monterey, CA 93943-5502; e-mail: golaz@nrlmry.navy.mil.

[1]COAMPS is a registered trademark of the Naval Research Laboratory.

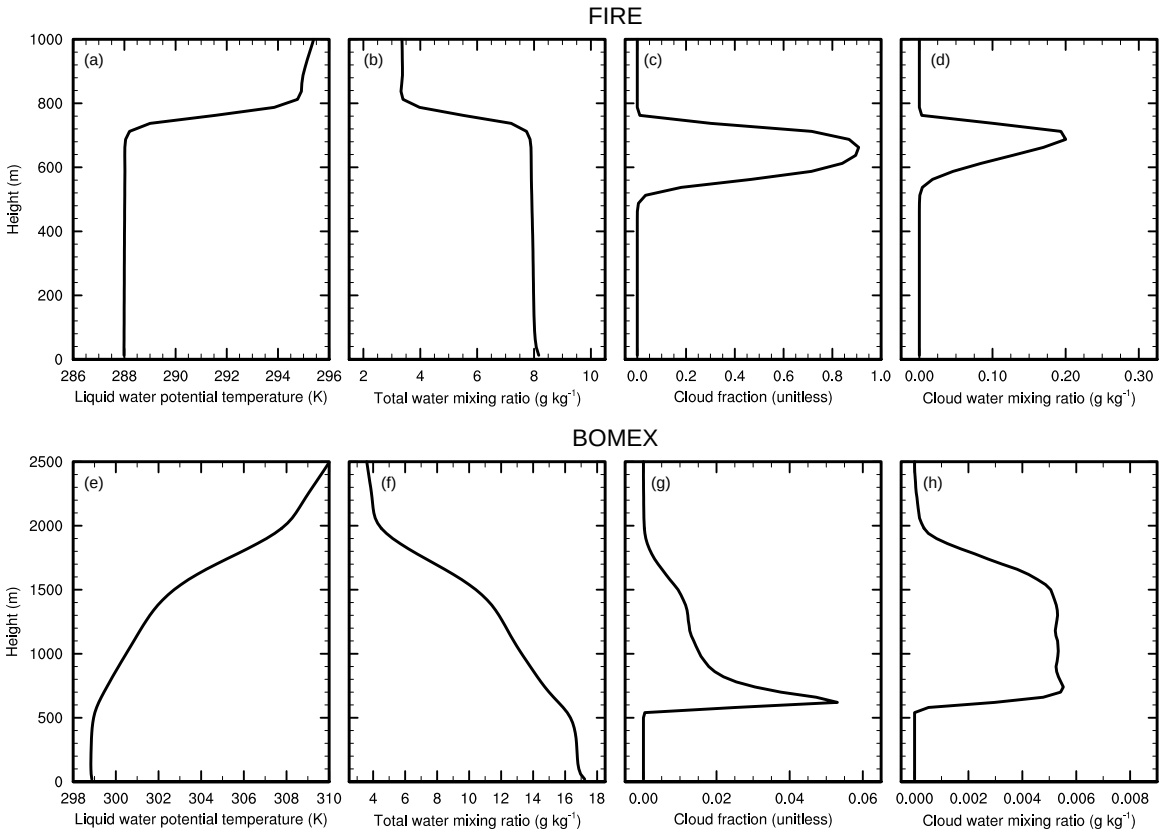

Figure 1: vertical profiles for the FIRE and BOMEX experiments: (a,e) liquid water potential temperature (θ_l), (b,f) total water mixing ratio (q_t), (c,g) cloud fraction, (d,h) cloud water mixing ratio (q_c).

1976):

$$\frac{\partial \overline{w'^2}}{\partial t} = \underbrace{-\bar{w}\frac{\partial \overline{w'^2}}{\partial z} - \frac{\partial \overline{w'^3}}{\partial z} - 2\overline{w'^2}\frac{\partial \bar{w}}{\partial z}}_{\text{Advection}} \underbrace{+\frac{2g}{\theta_0}\overline{w'\theta_v'}}_{\text{Buoyancy}} \underbrace{-\frac{2}{\rho_0}\overline{w'\frac{\partial p'}{\partial z}}}_{\text{Pressure}} \underbrace{-\epsilon_{ww}}_{\text{Dissipation}} \quad (1)$$

$$\frac{\partial \overline{w'^3}}{\partial t} = \underbrace{-\bar{w}\frac{\partial \overline{w'^3}}{\partial z} - \frac{\partial \overline{w'^4}}{\partial z} + 3\overline{w'^2}\frac{\partial \overline{w'^2}}{\partial z} - 3\overline{w'^3}\frac{\partial \bar{w}}{\partial z}}_{\text{Advection}} \underbrace{+\frac{3g}{\theta_0}\overline{w'^2\theta_v'}}_{\text{Buoyancy}} \underbrace{-\frac{3}{\rho_0}\overline{w'^2\frac{\partial p'}{\partial z}}}_{\text{Pressure}} \underbrace{-\epsilon_{www}}_{\text{Dissipation}} . \quad (2)$$

Because of the incompressibility assumption, these equations are not strictly valid for COAMPS-LES. However, they do provide useful guidance in interpreting budget terms. Budgets for the higher moments from numerical model are sometimes constructed by computing a number of terms appearing in Eqs (1)-(2) directly from the model fields, while inferring the remaining ones using a residual approach. This approach does not guarantee complete accuracy and consistency of the budget. Therefore, we prefer to follow an alternate approach in which we first construct an exact numerical budget (within machine precision) from the model numerics, and then relate the various contributions of that budget to terms appearing in Eqs (1)-(2). These budgets provide direct and exact contributions from the advection, buoyancy, pressure and dissipation terms, as well as the Robert time filter.

4.1 *Comparisons of* $\overline{w'^2}$, $\overline{w'^3}$, $\overline{Sk_w}$

First, we compare vertical profiles of domain-averaged resolved $\overline{w'^2}$, $\overline{w'^3}$ and skewness $\overline{Sk_w} \equiv \overline{w'^3}/\overline{w'^2}^{3/2}$ for FIRE and BOMEX (Fig. 2). Broadly speaking, $\overline{w'^2}$ can be interpreted as a measure of the vigor of the turbulence, whereas $\overline{w'^3}$ provides additional information about its organization. Small values of $\overline{w'^3}$ occur when the distribution of w is relatively symmetric between up and downdrafts regardless of the strength of the turbulence. Large positive values of $\overline{w'^3}$ indicate the dominance of strong and narrow updrafts and large negative values strong and narrow downdrafts. The skewness $\overline{Sk_w}$ is essentially a normalized measure of $\overline{w'^3}$.

The nature of the mixing is very different between FIRE and BOMEX. Turbulent motions in the FIRE case are generated by cloud-top radiative cooling. In BOMEX,

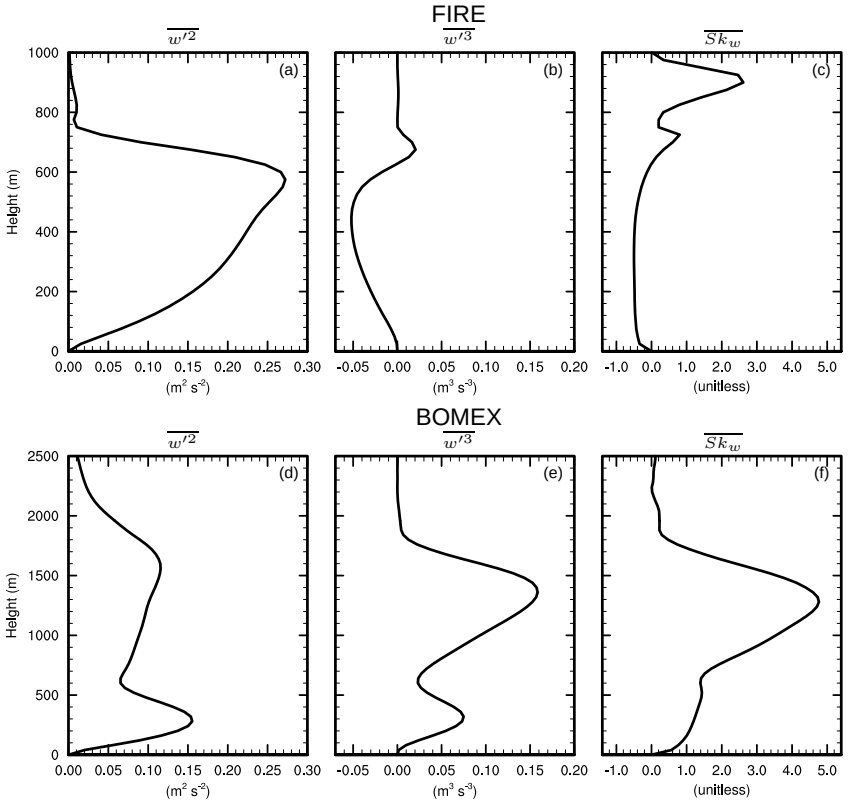

Figure 2: Vertical profiles of resolved $\overline{w'^2}$, $\overline{w'^3}$ and skewness ($\overline{Sk_w}$) the FIRE and BOMEX experiments.

they are generated by surface fluxes and conditional instability that leads to the formation of shallow cumulus clouds. This translates into markedly different w moments as shown in Fig. 2. The strength of the turbulence as measured by $\overline{w'^2}$ is greater for FIRE than BOMEX. The FIRE $\overline{w'^2}$ profile shows a single maximum in the cloud. In contrast, the profile from BOMEX exhibits one local maximum in the subcloud layer related to the eddies generated from the surface fluxes, and a second maximum in the cloud layer due to latent heat release.

Profiles of $\overline{w'^3}$ and $\overline{Sk_w}$ show an almost unskewed turbulent field for FIRE. The skewness has a nearly constant value of -0.5 in the lower portion of the mixed layer and a small positive maximum near cloud top. The larger maximum around 900 m is caused by small $\overline{w'^2}$ values in the denominator of $\overline{Sk_w}$ and has little physical relevance. The negative skewness in the mixed layer indicates slightly stronger and narrower downdrafts, which is consistent with cloud-top radiative driven turbulence.

A different picture emerges for BOMEX. $\overline{w'^3}$ and the skewness are positive throughout the entire boundary layer. The skewness reaches a large maximum of nearly 5 in the upper portion of the cloud layer. The cloud layer increase in skewness can be interpreted as updrafts becoming progressively stronger and narrower with height in accordance with the cloud core analysis of Siebesma et al. (2003).

4.2 $\overline{w'^2}$ *budgets*

The $\overline{w'^2}$ budget for FIRE and BOMEX are shown in Fig. 3. Terms shown shown are advection, buoyancy, pressure, dissipation, and time filter. The storage and the net (difference between the sum of all the terms and the actual model change during the analysis period) are very small and not shown. Also shown with the advection term is the resolved turbulent transport term as computed from the model field ($-\partial\overline{w'^3}/\partial z$). The buoyancy term is decomposed into contributions from up and downdrafts:

$$\overline{w'\theta'_v} = a\overline{w'\theta'_v}^u + (1-a)\overline{w'\theta'_v}^d \qquad (3)$$

where a is the updraft area and $\overline{(\quad)}^u$, $\overline{(\quad)}^d$ denote averages over the updraft, respectively downdraft, portion of the flow. This simple decomposition can be useful in interpreting the role of the buoyancy. For example, warm updrafts ($w'_u > 0$, $\theta'_{u,v} > 0$) and cold downdrafts ($w'_d < 0$, $\theta'_{d,v} < 0$) can both contribute positively to the buoyancy.

The $\overline{w'^2}$ FIRE budget is in many respects similar to the ones analyzed by Moeng (1986) for two stratus-topped boundary layers. The major terms are buoyancy, pressure and advection. The buoyancy acts as a source of turbulence throughout the boundary layer with the exception of the entrainment zone. The buoyancy flux decomposition reveals that both up and downdrafts contributions are positive throughout most of the boundary layer. This can occur when the perturbation virtual potential temper-

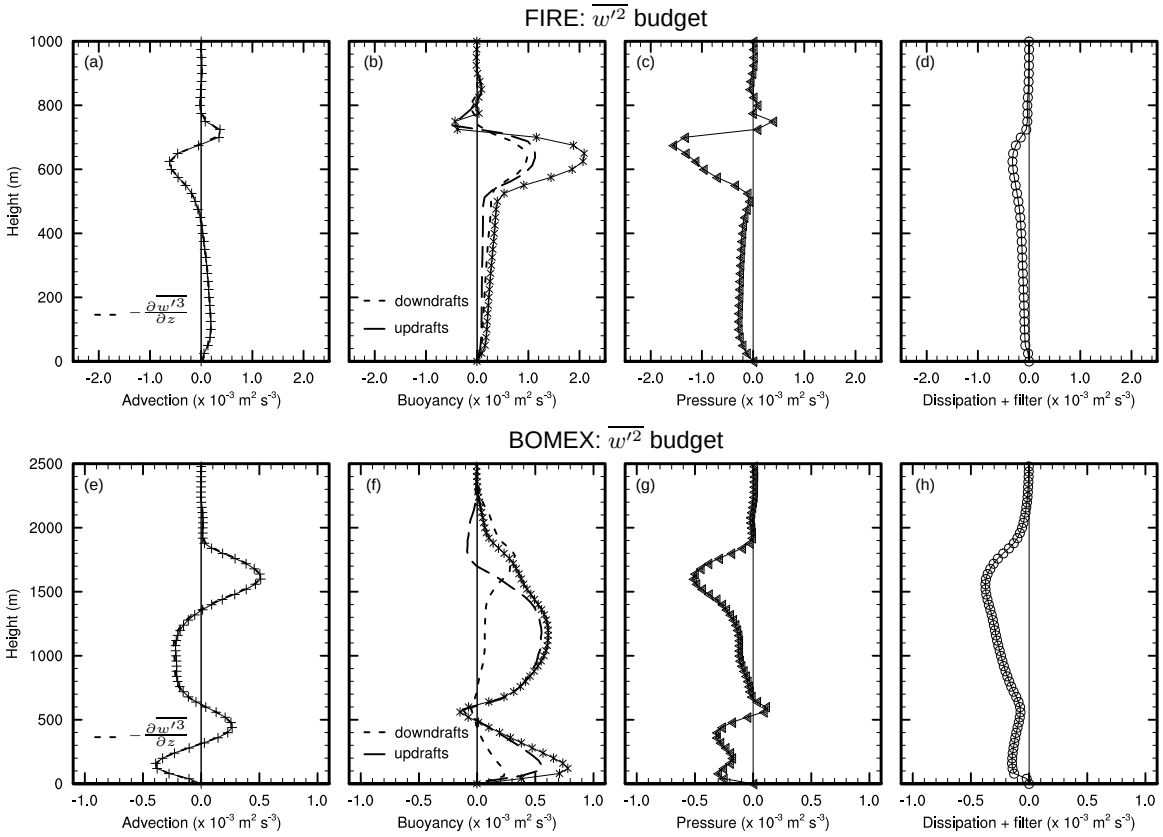

Figure 3: $\overline{w'^2}$ budget terms for the FIRE and BOMEX experiments: (a,e) advection term (line with crosses) and estimated transport term $-\partial\overline{w'^3}/\partial z$ (dashed line), (b,f) buoyancy term (line with stars), updrafts (long dashed line) and downdrafts (short dashed line) contributions to the buoyancy, (c,g) pressure term, (d,h) sum dissipation and time filter terms.

ature is positive in updrafts ($w'_u > 0$, $\theta'_{v,u} > 0$) and negative in downdrafts ($w'_d < 0$, $\theta'_{v,d} < 0$). Furthermore, up and downdrafts contribute nearly equally to the generation of turbulence, except in the entrainment zone. In this region, the updrafts are negatively buoyant and buoyancy becomes a sink of energy, whereas downdrafts do not contribute significantly.

The pressure term for FIRE (Fig. 3c) is the largest sink of $\overline{w'^2}$. It redistributes energy from the vertical to the horizontal directions. It peaks just below cloud top where updrafts are impeded in their ascend by the presence of the inversion and have their momentum diverted in the horizontal directions as a result. The advection term and the turbulent transport term $-\partial\overline{w'^3}/\partial z$ computed directly from the model fields show no visible differences (Fig. 3a). This term transports $\overline{w'^2}$ from the cloud layer into both the entrainment zone and the subcloud layer. The dissipation and time filter terms are comparatively small in magnitude and act to dissipate $\overline{w'^2}$.

The corresponding $\overline{w'^2}$ budget for BOMEX compares favorably with similar budgets from other shallow cumulus simulations discussed by Cuijpers et al. (1996) and de Roode and Bretherton (2003). As for FIRE, buoyancy is the major source of kinetic energy, except in a shallow region near cloud base where subcloud driven updrafts decelerate before undergoing renewed acceleration due to latent heat release in the cloud. The up and downdraft decomposition reveals that the buoyancy production is largely dominated by the updrafts from the surface up to 1600 m ($w'_u > 0$, $\theta'_{v,u} > 0$). Between 1700 m and the domain cloud top, updrafts become negatively buoyant ($w'_u > 0$, $\theta'_{v,u} < 0$). They consume their kinetic energy by overshooting into the inversion layer. The generation of turbulence in this layer is dominated by downdrafts ($w'_d < 0$, $\theta'_{v,d} < 0$) generated by evaporative cooling. In contrast to FIRE, the pressure and dissipation terms have comparable magnitudes. Because of the absence of a very strong inversion, there is less redistribution of energy from the vertical to the horizontal motions by the pressure term. The advection term is also relatively large. It mainly acts by transporting energy from the lower half to the upper half of the subcloud layer, and again from the lower portion to the upper portion of the cloud layer.

4.3 $\overline{w'^3}$ budgets

The FIRE and BOMEX $\overline{w'^3}$ budgets are plotted in Fig. 4. Shown along with the advection are two terms com-

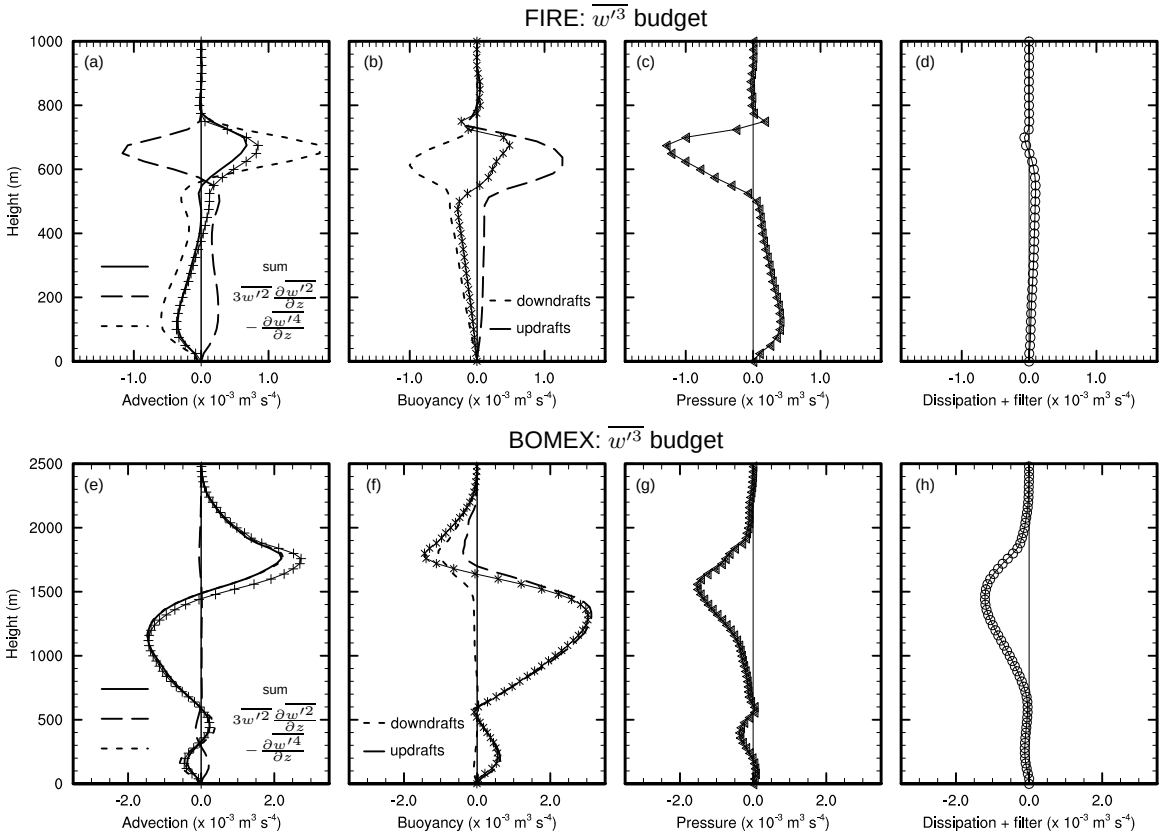

Figure 4: $\overline{w'^3}$ budget terms for the FIRE and experiments: (a,e) advection term (line with crosses), estimated transport term $-\partial\overline{w'^4}/\partial z$ (short dashed line), estimated turbulent production term $3\overline{w'^2}\partial\overline{w'^2}/\partial z$ (long dashed line) and their sum (solid line), (b,f) buoyancy term (line with stars), updrafts (long dashed line) and downdrafts (short dashed line) contributions to the buoyancy, (c,g) pressure term, (d,h) sum of dissipation and filter terms.

puted directly from Eq. (2): the turbulence advection ($-\partial\overline{w'^4}/\partial z$) and turbulence production ($3\overline{w'^2}\partial\overline{w'^2}/\partial z$). The buoyancy is again decomposed into up and downdrafts contributions:

$$\overline{w'^2\theta'_v} = a\overline{w'^2\theta'_v}^u + (1-a)\overline{w'^2\theta'_v}^d. \qquad (4)$$

In contrast to Eq. (3), the sign of $\overline{w'^2\theta'_v}^u$ and $\overline{w'^2\theta'_v}^d$ is essentially governed by the sign of the temperature perturbations ($\theta'_{v,u}$, $\theta'_{v,d}$), but its magnitude is influenced by the strength of the turbulence (w'^2_u and w'^2_d).

The largest terms in the FIRE budget are advection, buoyancy and pressure. The buoyancy, which consists of a positive contribution from the updrafts and a negative one from the downdrafts, changes sign at 580 m corresponding approximately to cloud base. The negatively buoyant downdrafts ($w'^2_d > 0$, $\theta'_{v,d} < 0$) generated by cloud top cooling dominate the buoyancy below cloud base, whereas the latent heat release in the updrafts is dominant inside the cloud layer ($w'^2_u > 0$, $\theta'_{v,u} > 0$). The pressure term acts to dissipate $\overline{w'^3}$ except in a shallow layer between cloud base (580 m) and 620 m where $\overline{w'^3}$ and the pressure term have the same sign.

The sum of the estimated contribution from the turbulent transport term ($-\partial\overline{w'^4}/\partial z$) and the turbulent production term ($3\overline{w'^2}\partial\overline{w'^2}/\partial z$) matches the advection term very well in the subcloud layer, but is a little bit smaller in the cloud layer (Fig. 4a). This could be due to the fact that these terms do not correspond exactly to the transport and production terms "seen" by the model due to numerical finite difference approximations. Nevertheless, the sum is close enough for the decomposition to be meaningful. It reveals that turbulence transports $\overline{w'^3}$ from the subcloud to the cloud layer and is countered by the production term which has opposite sign.

Cuijpers et al. (1996) analyzed a $\overline{w'^3}$ budget from another simulation of shallow cumulus clouds which shows fairly similar characteristics to ours. In contrast to FIRE, the BOMEX $\overline{w'^3}$ budget is dominated by production due to buoyancy. Between the surface and 1700 m, the buoyancy term consists almost exclusively of contributions from the updrafts, and above that level the situation is reversed. Downdrafts generated by evaporative cooling in the inversion layer account for most of the buoyancy term there. The advection term is dominated by the turbulence transport term ($-\partial\overline{w'^4}/\partial z$) which transports ($\overline{w'^3}$) from the lower portion to the upper portion of the cloud layer. The production term $3\overline{w'^2}\partial\overline{w'^2}/\partial z$ only plays a minor role in the subcloud layer. Pressure, dissipation, and

time filter all act to dissipate $\overline{w'^3}$ and tend to be largest near the top of the cloud layer.

5. CONCLUSION

Exact numerical budgets of the second and third moment of the vertical velocity have been obtained from COAMPS-LES. They reflect fundamental differences in the turbulence dynamics. Extreme cases are on the one hand the nighttime stratocumulus (FIRE) driven by cloud top radiative cooling, and on the other hand the trade-wind cumulus layer of BOMEX driven by surface fluxes and conditional instability of the atmosphere. The third moment of the vertical velocity ($\overline{w'^3}$) and the skewness are relatively small for the stratocumulus and large for the cumulus layer. The vertical velocity distribution is therefore relatively symmetric for FIRE, but positively skewed for BOMEX with the presence narrow and strong updrafts balanced by broad and weak downdrafts. This can be explained by the derived ($\overline{w'^3}$) budgets, and in particular by the buoyancy production term. In BOMEX, it is positive from the surface up to the level of neutral buoyancy and becomes negative above that level. Below that level the buoyancy is dominated by contributions from the positively buoyant updrafts with the downdrafts having almost no effect. However, above the level of neutral buoyancy, the negatively buoyant downdrafts generated by evaporative cooling dominate the buoyancy. The situation is quite different in the stratocumulus case. First, the magnitude of the buoyancy term is much smaller than for the cumulus layer. Second, the buoyancy is negative from the surface to cloud base and positive in the cloud layer. Both updrafts and downdrafts contribute significantly to the buoyancy throughout the boundary layer. Their contributions have similar magnitude but opposite signs. Downdrafts are always negative and dominate below cloud base. Updrafts, which are always positive dominate in the cloud layer. This leads to a partial cancellation and results in a buoyancy term that is much smaller than in BOMEX.

6. ACKNOWLEDGMENTS

This work was performed while the first author held a National Research Council Research Associateship Award at the Naval Research Laboratory, Monterey, California. Shouping Wang was supported by the Office of Naval Research and the Naval Research Laboratory through CBLAST project.

7. REFERENCES

André, J. C., G. de Moor, P. Lacarrère, and R. du Vachat, 1976: Turbulence approximation for inhomogeneous flows: Part I. The clipping approximation. *J. Atmos. Sci.*, **33**, 476–481.

Bott, A., 1989: A positive definite advection scheme obtained by nonlinear renormalization of the advective fluxes. *Mon. Wea. Rev.*, **117**, 1006–1015.

Cuijpers, J. W. M., P. G. Duynkerke, and F. T. M. Nieuwstadt, 1996: Analyses of variance and flux budgets in cumulus-topped boundary layers. *Atmos. Res.*, **40**, 307–337.

de Roode, S. R. and C. S. Bretherton, 2003: Mass-flux budgets of shallow cumulus clouds. *J. Atmos. Sci.*, **60**, 137–151.

Golaz, J.-C., V. E. Larson, and W. R. Cotton, 2002: A PDF based model for boundary layer clouds. Part I: Method and model description. *J. Atmos. Sci.*, **59**, 3540–3551.

Grant, A. L. M. and A. R. Brown, 1999: A similarity hypothesis for cumulus transports. *Quart. J. Roy. Meteor. Soc.*, **125**, 1913–1935.

Grant, A. L. M. and A. P. Lock, 2004: The turbulent kinetic energy budget for shallow cumulus convection. *Quart. J. Roy. Meteor. Soc.*, **130**, 401–422.

Hodur, R. M., 1987: The Naval Research Laboratory's Coupled Ocean/Atmosphere Mesoscale Prediction System (COAMPS). *Mon. Wea. Rev.*, **125**, 1414–1430.

Klemp, J. B. and R. B. Wilhelmson, 1978: The simulation of three-dimensional convective storm dynamics. *J. Atmos. Sci.*, **35**, 1070–1095.

Lappen, C.-L. and D. A. Randall, 2001: Toward a unified parameterization of the boundary layer and moist convection. Part I: A new type of mass-flux model. *J. Atmos. Sci.*, **58**, 2021–2036.

Moeng, C.-H., 1986: Large-eddy simulation of a stratus-topped boundary layer. Part I: Structure and budgets. *J. Atmos. Sci.*, **43**, 2886–2900.

Moeng, C.-H., W. R. Cotton, C. Bretherton, A. Chlond, M. Kairoutdinov, S. Krueger, W. S. Lewellen, M. K. MacVean, J. R. M. Pasquier, H. A. Rand, A. P. Siebesma, B. Stevens, and R. I. Sykes, 1996: Simulation of a stratocumulus-topped planetary boundary layer: Intercomparison among different numerical codes. *Bull. Amer. Meteor. Soc.*, **77**, 261–278.

Siebesma, A. P., C. S. Bretherton, A. Brown, A. Chlond, J. Cuxart, P. G. Duynkerke, H. Jiang, M. Khairoutdinov, D. Lewellen, C.-H. Moeng, E. Sanchez, B. Stevens, and D. E. Stevens, 2003: A large eddy simulation intercomparison study of shallow cumulus convection. *J. Atmos. Sci.*, **60**, 1201–1219.

Stull, R. B., 1988: *An Introduction to Boundary Layer Meteorology*. Kluwer Academic Publishers, 666 pp.